Journal of ELECTRICAL ENGINEERING, VOL 55. NO 10/S, 2004, 73-76

INVESTIGATION IN DETECTION OF FATIGUE CRACKS UNDER RIVET HEAD AIRFRAME USING IMPROVED GMR MAGNETOMETER IN AN EDDY CURRENT SYSTEM

L. Perez[*] — J. Le Hir[*,] — C. Dolabdjian[*] — L. Butin[**]**

We have designed and built a magnetic imaging system associated with eddy current technique for quantitative analysis of the fatigue cracks under rivet of air craft aluminum alloys in planar structures. Sensor utilizes Improved Giant MagnetoResistance Magnetometer (IGMRM) which measures the magnetic field mainly induced by eddy currents distribution. It consists on a mono-axis IGMRM, coil inductors, computer controlled *x*-*y*-*z* stage, data acquisition and analysis software. The laboratory setup can scan planar samples with dimensions of up to 30 cm*5 cm*5 cm, with an optimal spatial resolution and repeatability of around 1 µm, a magnetic field sensitivity of $(5/\sqrt{f})$ nT/√Hz and a dynamic of (127+10 Log(*f*)) dB/√Hz (where *f* is here the induced current frequency), which, respectively, saturate to an optimal value of around 50 pT/√Hz and 166 dB/√Hz. In this article, we report the design and technical issues related to the inspection system, and outline preliminary results in detection of fatigue cracks under rivet head airframe.

Keywords: GMR, magnetometer, low noise, eddy current

1 INTRODUCTION

Over the last years, there has been an increased interest for detecting fatigue cracks within assembled structures in the aging aircraft NDE community. The detection of deep and small cracks initiating within the bore of multi-layered structures without removing rivets still represents a significant problem. In particular, second and third-layer flaw detection is a challenge for any of the NDE inspection methods currently in use [1]. Recent advances in magnetic sensor technology made the electromagnetic NDE evaluation method very attractive to address this difficult problem [2]. In this way, we present eddy current inspection systems which incorporates improved GMR magnetometer [3]. The approach is comparable to the current state-of-the-art [4, 5, 6]. However, the IGMRM, as developed and used here, enhances eddy current system detection potential in the scope of SQUID system [4, 7]. The experimental configuration developed is explained and its performances are given along with experimental results for detection of typical EDM (Electrical Discharge Machined) notches at riveted joints in multilayer aluminum alloy sample. Some digital image processing is used to improve defect detection.

2 EDDY CURRENT SYSTEM DESCRIPTION

The Eddy Current System (ECS) consists on the combination of an IGMRM [3, 8] and a classical inductor, which, generally, surrounds the magnetometer. A view of the head of detection is given in figure 1. The sensing axis is in plane or orthogonal of the sample plan. The performances of the magnetometer are summarized in table I and complementary information will be found in [3]. The inductor coil is changeable and permits to generate a high induce current density $J_{x,y,z}$ in the sample higher than 10^4 A/m^2 on aluminum sample conductivity σ_{al} of about 25 MS/m. Penetration depth is governed by the skin-depth relationship:

$$\delta = \sqrt{\frac{2}{\omega_0 \mu \sigma}} \approx \frac{0.1}{\sqrt{f_0}} \text{m} \approx 10\text{mm}\Big|_{f_0=100\text{Hz}} \qquad (1)$$

where ω_0, μ are, respectively, the induced current angular frequency and the material permeability.

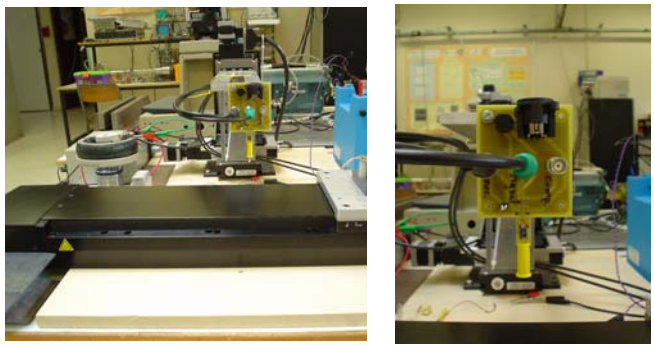

Fig. 1. Photos of the full ECS and details

The very high dynamic and intrinsic noise of this ECS are compatible with laboratory and industrial open environment operation. The usual noise level of our lab during operation is around 1 nT/√Hz until 50 Hz and decreases at higher frequency. This environmental noise measurement will be reduced by using gradiometric structures or averaging, but preliminary results show that the high intrinsic dynamic of the ECS is able to compensate this measurement degradation. An experimental benchmark was developed to assess the feasibility of the ECS. Two calibrated defects were machined near rivet hear frame (see Fig. 3). A sinusoidal current source provides a current through the inductor of controlled amplitude and frequency f_0 ($\omega_0 = 2\,\pi\,f_0$). The magnetometer detects, in this confi-guration, the in-phase

[*] GREYC - CNRS UMR 6072 - Université de Caen & ENSICAEN - 6, Bd du Maréchal Juin - 14050 Caen Cedex, E-mail: C.Dolabdjian@greyc.ismra.fr
[**] CEGELEC CNDT - ZI du bois des Bordes - 91229 Bretigny S/Orge Cedex

ISSN 1335-3632

and out-phase magnetic field image ($B_{\text{in-phase}}$ and $B_{\text{out-phase}}$) distorted by sample and defects in the plane of the displacement near the inspected surface.

Table 1: Improved GMR magnetometer performances (*Experimental measurement limited by the reference)

Supply voltage	± 12 V
First stage gain output sensitivity (T_r)	≈ 1,000 V/T
Bandwidth (Bd)	dc to > 300 kHz
Slew-rate (S_r)	Theoretical > 160 T/s Measured >37.5 T/s*
Distortion (Total Harmonic Distortion) f = 10 Hz - 1 kHz	Amplitude: ± 1mT$_{peak}$ < 0.03 %* Theoretical : < 0.001%
Noise density ($b_{\text{sensor noise}}(t)$)	5/√f nT/√Hz f< 1 kHz ≈ 50 pT/√Hz f> 1 kHz
Dynamic f = 10 Hz - 100 Hz - 1 kHz	143 - 153 - 163 dB/√Hz
Full Scale field range	± 12 mT
Spatial resolution	< 1 mm Mainly, limited by the encapsulation
Hysteresis	Negligible
Perpendicular field sensitivity	Cos(β)
Operating temperature range	-40°C to + 85°C
Insensitivity to magnetic shock	> 40 mT
Encapsulated sensor external size	0.7 mm× 0.7 mm× 4 mm

Output sensor voltage amplitude $V_{\text{out}} \equiv V_{\text{out}}(\omega_0, x, y, z, t)$ is

$$V_{out} = T_r(B_{\text{in-phase}} + B_{\text{offset-in}})Cos(\omega_0 t) + \\ + T_r(B_{\text{out-phase}} + B_{\text{offset-out}})Sin(\omega_0 t) + e_n(t) \quad (2)$$

with $B_{\text{in-phase}}(\omega_0, x, y, z, t)$ and $B_{\text{out-phase}}(\omega_0, x, y, z, t)$ and where $B_{\text{offset-in}}$ and $B_{\text{offset-out}}$ are respectively magnetic component induced by conducting sample proximity. Here x, y, z is the 3D spatial position.

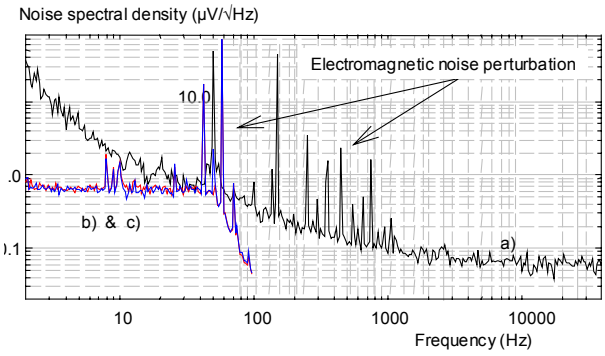

Fig. 2. Output intrinsic voltage spectral density of the sensor in laboratory open environment a) and both output power spectral density of the ECS $v_n'(t)$ and $v_n''(t)$ (f_0 = 200 Hz & post detection bandwidth = 50Hz) b) & c)

The power spectral density $e_n(t)$ is defined by:

$$\overline{e}_n^2(t) = T_r^2 \begin{pmatrix} \overline{b}^2_{\text{env-noise}}(t) + \overline{b}^2_{\text{sensor-noise}}(t) \\ + \overline{b}^2_{\text{inductor}}(t) + \overline{e}^2_{\text{amplifier}}(t) \end{pmatrix} \quad (V_{eff}^2 / Hz) \quad (3)$$

where $b_{\text{env-noise}}$, $b_{\text{sensor-noise}}$, b_{inductor}, $e_{\text{amplifier}}$ are, respectively, magnetic environmental noise, intrinsic sensor noise, induced current source generator noise and amplifier noise. Using a synchronous demodulator at ω_0 pulsation, we are able to evaluate the in-phase and out-phase voltage amplitudes of the detected signal:

$$V_{\text{in-phase}} = T_r k_{\text{dec}}(B_{\text{in-phase}} + B_{\text{offset-in}}) + v_n'(t) \\ V_{\text{out-phase}} = T_r k_{\text{dec}}(B_{\text{out-phase}} + B_{\text{offset-out}}) + v_n''(t) \quad (4)$$

where the power spectral density of $v_n'(t)$ and $v_n''(t)$ are given by:

$$\overline{v}_n''^2(t) = k_{\text{dec}}^2 T_r^2 \begin{pmatrix} \overline{b}^2_{\text{env-noise}}(f_0) + \overline{b}^2_{\text{sensor-noise}}(f_0) \\ + \overline{b}^2_{\text{inductor}}(f_0) + \overline{e}^2_{\text{amp+SunD}}(f_0) \end{pmatrix} \quad (5)$$

$$\overline{v}_n''^2(f_0) = \eta^2(f_0) \qquad (V_{\text{eff}}^2 / \text{Hz})$$

where $e_{\text{amp+SynD}}$ is the summation of the power spectral density of amplifier noises, k_{dec} is a coefficient that depends on the synchronous detector.

Table 2: Intrinsic noise level and dynamic of the ECS using IGMRM ($0.1 < f_0 < 1$ kHz).

	Highest voltage spectral density of the ECS (nV/√Hz)	Output dynamic of measurement (f_0 = 100 Hz, Δf=1 Hz) (dB/√Hz)
$\overline{v}_{\text{in-phase}}(f_0)$, $\overline{v}_{\text{out-phase}}(f_0)$	$\eta(f_0)\Delta f = 5\, k_{dec} T_r \frac{\Delta f}{\sqrt{f_0}}$	$\frac{2 \cdot 12 \cdot 10^9 \sqrt{f_0}}{5\, k_{dec} T_r \Delta f} \approx 140$
$\overline{v}_{\text{mod}}(f_0)$	$\sqrt{2}\eta(f_0)\Delta f = \sqrt{2}\, 5\, k_{dec} T_r \frac{\Delta f}{\sqrt{f_0}}$	$\frac{2 \cdot 12 \cdot 10^9 \sqrt{f_0}}{5\, k_{dec} T_r \Delta f} \approx 140$
	Highest phase spectral density of the ECS (rad/√Hz)	Maximal Signal-to-Noise-Ratio of measurement (f = 100 Hz, Δf=1 Hz) (dB/√Hz)
$\overline{\varphi}_{\text{mod}}(f_0)$	$\eta(f_0)\Delta f = 1.2 \cdot 5\, k_{dec} T_r \frac{\Delta f}{\sqrt{f_0}}$	$\frac{\pi\sqrt{f_0}}{1.2 \cdot 5\, k_{dec} T_r \Delta f} 10^9 \approx 120$

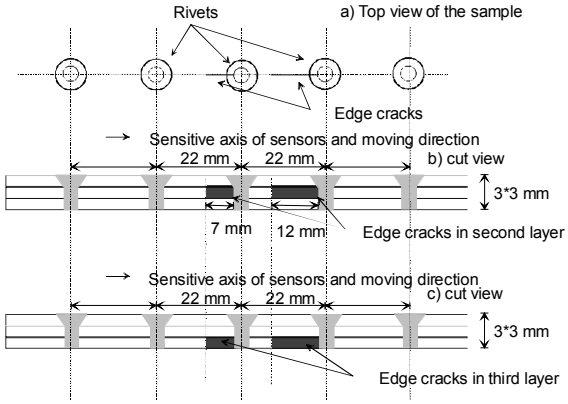

Fig. 3. Top view and cut view of sample.

In open laboratory magnetic noise environment, the figure 2 presents $\overline{v_n'(t)}^2$ and $\overline{v_n''(t)}^2$ output ECS power spectral voltage density of around 0.6 µV/√Hz (in 50 Hz output bandwidth) with f_0 = 200 Hz, measurements were made with HP3652A analyser. The transfer T_r, K_{dec} are respectively equal to 1000 V/T and 2). They fit with the excepted value. Expected expressions of amplitude and associated voltage noise versus Δf post-detection band-width, in low magnetic noise environment, ($v_n << T_r\, k_{\text{dec}}\, B_{\text{in-phase,out-phase}}$ and $\Delta f << f_0$) can be evaluated and is resumed in table 2.

As currently used in NDE processes, different kinds of signal representations uses demodulated signals and classical Lissajous curves, reel, imaginary, modulus, and phase versus the position or time as presented in results part. The maximal dynamic of the ECS is for previous description given in table 2. It shows very high intrinsic ECS dynamic and its performances are very comparable to the state of the art of SQUID system [4], when the noise respects conditions given in previous paragraph.

3 EXPERIMENTAL INVESTIGATION

Multilayer samples consist on 3 layers of 2024 T3 Aluminum (3 mm tick), as shown in figure 3, with 4 mm diameter holes containing ASNA2019/Ti40 15 rivets [9].

Experimental results of detection were given for (12 mm and 7 mm length and ≈ 100 µm width) EDM notches under rivets compare to healthy rivets. ECS is installed on X, Y Z scanner. It consists on 3 translation stages with high position precision and high repeatability.

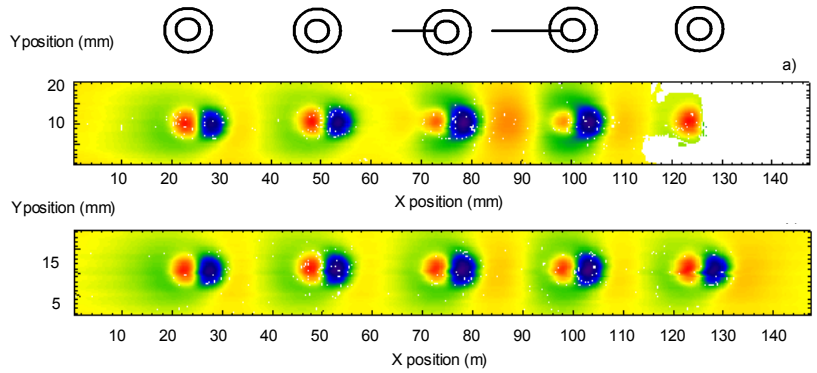

Fig. 4. Magnetic image scan of the out-phase amplitude, defects appearing in second layer a) in third layer b), as presented in figure 3.

The magnetic scanning image variable used is usual. These performances could be adapted and improved to assess detection feasibility. Nevertheless, the inductor geometry associated to the IGMRM, size defects and defect signal amplitude limit, at present, the spatial characteristics of the detection.

4 RESULTS

The environmental noise and the dynamic of the eddy current generator give an equivalent magnetic noise lower than 1 nT/√Hz at 100 Hz (see figure 2). It degrades intrinsic dynamic of the system of around 10 dB. We present in figure 4, after a post processing tilt and lift off compensation, the magnetic images of out-phase components. Equivalent fatigue cracks appear distinctly on both measurements.

The out-phase amplitude versus a single X scanning centered on the rivets is presented in figure 5 and 6 (for 500 µm resolution). Each figure cracks appear distinctly. The gain field to voltage transfer is equal to around 10^5 V/T. The induced current amplitude and frequency are around 35 mA_{eff} and 100 Hz. The maximal dynamic amplitude of the detection, in previous conditions, is for the 12 mm and 7 mm defect length, respec-tively of $(0.06/(3\ \mu V_{eff}/\sqrt{Hz}*35mA_{eff})$ = 115 dB/√Hz/A and 111 dB/√Hz/A.

It corresponds to 85 dB and 82 dB, respectively, with our induced eddy current amplitude of 35 mA_{eff} in 1 Hz

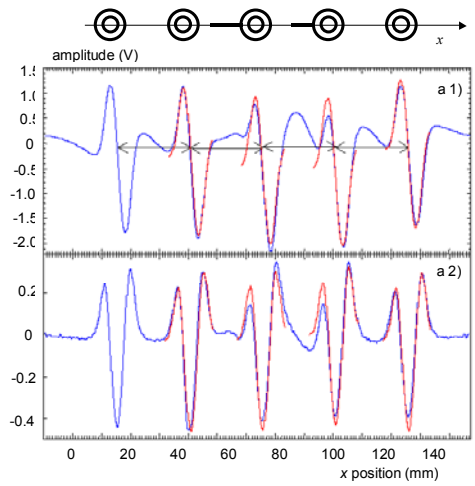

Fig. 5. Magnetic image scan of the out-phase amplitude, defects appearing in second layer a), as presented in figure 4.

bandwidth for the second layer. Similarly, for the third layer, we obtain maximal signal to noise ratio higher than 80 dB/√Hz/A.

More information can be obtain by analyzing the derivative curve of the out-phase voltage amplitude versus the X scanning as given in Fig. 4.

We can notice the symmetric response, around the center rivet position, in all healthy rivet cases. Meanwhile, up to 20-40 dB/√Hz/A, signal fluctuations are observed around damaged rivets in Fig. 6. It is induced by geometric fluctuation or lift off variation.

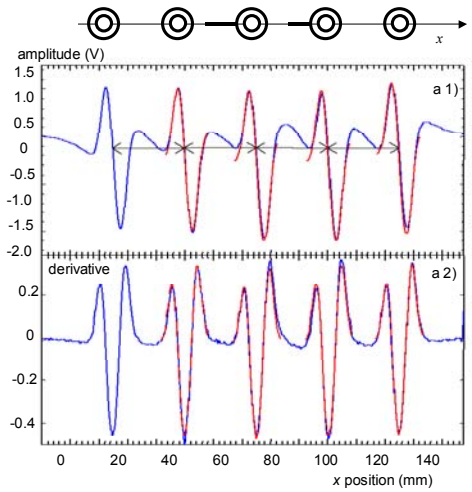

Fig. 6. Magnetic image scan of the out-phase amplitude, defects appearing in third layer b), as presented in figure 4.

More, by using improved image processing, it's possible to improve the visualization of healthy rivets. One result, using computing face symmetry and threshold [10, 11], is presented in Fig. 7.

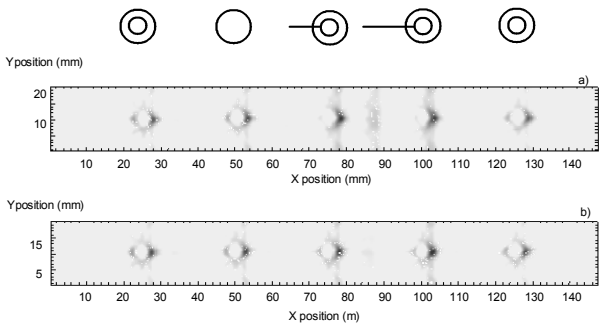

Fig. 7. Magnetic image scan of the out-phase amplitude after image processing, defects appearing in second layer (full scale threshold 30 %) a) in third layer (full scale threshold 30 %) b), as presented in Fig. 4.

4 CONCLUSIONS

Successful defect detection of fatigue cracks under rivet head frame was shown as example in which IGMRM sensors are used in eddy current NDE applications. In this first part of research, we were, mainly, interested in the ability of ECS detection. High resolutions scans show that notch detection could be notably improved with low Signal to Noise Ratio degradation or much industrial adapted spatial resolution. For this last purpose, coupling IGMRM with much optimized excitation schemes enable deeper and stronger detection criterions and so offer the potential to solve a wider range of NDE problems. Indeed, the combination of a sensor's high field sensitivity and sophisticated excitation geometry could be key in detecting small and deep-laying material defects.

Acknowledgement

This work was partly supported by European Regional Development Fund (FEDER) and French National Territories Development Fund (FNADT).

REFERENCES

[1] T. Dogaru, S. Smith, "Novel eddy current probes for detection of deep cracks around fastener holes", Aging Aircraft 2001, Orlando, Sept. 10-13(2001)
[2] C. Smith, R. Schneider, "Low field magnetic sensing with GMR sensors", Sensors-Expo, Baltimore, may, 1999
[3] L. Perez, C. Dolabdjian, G. Waché, L. Butin, "Advance in magnetometer performances applied in eddy current sensor array", WCNDT'04 Montréal, August 28-31(2004)
[4] H. Krause, M. Kreutzbruck, "Recent SQUID development in NDE", Physica C(368), 70-79(2002)
[5] C. Smith, R. Schneider, T. Dogaru, S. Smith, "GMR Magnetic sensor Arrays for NDE Eddy-current Testing", Review of progress in quantitative NDE, Vol. 657(1), AIP, 419, 2003
[6] R. Smith, G. Hugo, "Deep corrosion and crack detection in aging aircraft using transient Eddy current NDE", Aging Aircraft 2001, Orlando, Sept. 10-13(2001)
[7] M. Kreutzbruck, K. Allweins, G. Gierelt, H. Krause, S. Gärtner, W. Wolf, "Defect detection in thick aircraft samples using HTS SQUID magnetometers, Physica C(368), 85-90(2002)
[8] G. Waché, L. Butin, L. Perez, C.Dolabdjian, "New perspectives with magnetoresistance array technologies from research to industrial applications", WCNDT'04 Montréal
[9] Ateliers de Haute Garonne, Ets AURIOL & Cie, S.A. Z.I. Flourens, BP3 31130 Flourens Cedex, FRANCE
[10] P. Kovesi, "Image Feature from phase Congruency", Videre : A", Journal of Computer Vision Research, MIT press, Volume(1)3, (1999)
[11] J. Le Hir, GREYC-CEGELEC CNDT, Internal report (2004)

Received 28 June 2004

Laurent Perez (Ing) was born in 1969 in France. He is graduated from CNAM of Caen in physics and instrumentation. Interests: instrumentation and computer aided measurements.

Jérome Le Hir (Ing) was orn in 1980 in France. He received master of science level at school of engineering CPE Lyon (2004, France), topics: electronics, telecommunications and computer science. Former graduate student exchange at Oregon State University (USA), college of electrical engineering. Interests: digital signal and image processing.

Christophe Dolabdjian (Pr) was born in France, in 1967. He received the MS and the PhD degree in electronics and instrumentation and the Habilitation Diploma, from the University of CAEN, France, in 1991, 1994, 2000, respectively. He has been a professor of electronics, since 2001, at the University of CAEN. His research interests included studies, improvement, development and comparison of numerous very high sensitivity and very low magnetic noise sensors, as well as the development and studies in open or shielded environment applications.

Laurent Butin (Dr) was born in 1969, in France. He is graduated of master of sciences university of Paris VII Jussieu. He received PhD degree in 3D ultrasonic (UT) modelization at the French Atomic Commission (CEA). He was an UT technical manager at RD-TECH (1999-2002) and responsible of technologies and engineer service at Cegelec-CNDT since 2002.